Investigation of Interfacial Charge Transfer in Solution Processed Cs2SnI6 Thin Films

著者	Kapil Gaurav, Ohta Takeshi, Koyanagi Tsuguo, Vigneshwaran Murugan, Zhang Yaohong, Ogomi Yuhei, Pandey Shyam S., Yoshino Kenji, Shen Qing, Toyoda Taro, Rahman Md. Mijanur, Minemoto Takashi, Murakami Takurou N., Segawa Hiroshi, Hayase Shuzi
journal or publication title	The Journal of Physical Chemistry C
volume	121
number	24
page range	13092-13100
year	2017-06-22
URL	http://hdl.handle.net/10228/00006836

doi: info:doi/10.1021/acs.jpcc.7b04019

Investigation of Interfacial Charge transfer in Solution Processed Cs_2SnI_6 Thin Films

Gaurav Kapil,[†] Takeshi Ohta,[‡] Tsuguo Koyanagi,[‡] Murugan Vigneshwaran,[‡] Yaohong Zhang,[χ] Yuhei Ogomi,[‡] Shyam S Pandey,[‡] Kenji Yoshino,[§] Qing Shen,[χ] Taro Toyoda,[χ] Md. Mijanur Rahman,[ψ] Takashi Minemoto,[ψ] Takurou N. Murakami,[ϒ] Hiroshi Segawa,[†] Shuzi Hayase[‡]*

[†]The University of Tokyo, Research Center for Advanced Science and Technology, 4-6-1, Komaba, Meguro-ku, Tokyo 153-8904, Japan

[‡]Kyushu Institute of Technology, Graduate School of Life Science and Systems Engineering, 2-4 Hibikino, Wakamatsu-ku, Kitakyushu 808-0196 Japan

[§]University of Miyazaki, Faculty of Engineering, Gakuen-kibanadai-nishi-1-1, Miyazaki, 889-2192, Japan

[χ]University of Electro Communication, Graduate school of Informatics and Engineering, 1-5-1 Chofugaoka, Chofu, Tokyo, 182-8585, Japan

[ψ]Ritsumeikan University, Department of Electrical and Electronic Engineering , 1-1-1 Nojihigashi, Kusatsu, Shiga 525-8577, Japan

[ϒ]The National Institute of Advanced Industrial Science and Technology, 1-1-1 Higashi, Tsukuba, Ibaraki 305-8565, Japan

E-mail: kapil@dsc.rcast.u-tokyo.ac.jp

KEYWORDS: Cs_2SnI_6, Lead free perovskite, Transient absorption spectroscopy, Interface charge transfer.

ABSTRACT

Cesium tin halide based perovskite Cs_2SnI_6 has been subjected to in-depth investigations owing to its potentiality towards the realization of environment benign Pb free and stable solar cells. In spite of the fact that Cs_2SnI_6 has been successfully utilized as an efficient hole transport material owing to its p-type semiconducting nature, however, the nature of the majority carrier is still under debate. Therefore, intrinsic properties of Cs_2SnI_6 have been investigated in detail to explore its potentiality as light absorber along with facile electron and hole transport. A high absorption coefficient ($5 \times 10^4\ cm^{-1}$) at 700 nm indicates the penetration depth of 700 nm light to be 0.2 μm which is comparable to conventional Pb based solar cells. Preparation of pure and CsI impurity free dense thin films with controllable thicknesses of Cs_2SnI_6 by solution processable method has been reported to be difficult owing to its poor solubility. An amicable solution to circumvent such problems of Cs_2SnI_6 has been provided utilizing spray-coating in combination of spin coating. Presence of two emission peaks at 710 nm and 885 nm in the prepared Cs_2SnI_6 thin films indicated co-existence of quantum dot and bulk parts which were further supported by transmission electron microscopy (TEM) investigations. Time resolved photoluminescence (PL) and transient absorption spectroscopy (TAS) were employed to investigate the excitation carrier lifetime, which revealed fast decay kinetics in the pico seconds (ps) to nano seconds (ns) time domains. Time resolved microwave photoconductivity decay (MPCD) measurement provided the mobile charge carrier life time exceeding 300 ns which was also in agreement with the nanosecond transient absorption spectroscopy (ns-TAS) indicating slow charge decay lasting up to 20μs. TA assisted interfacial charge transfer investigations utilizing Cs_2SnI_6 in combination with n-type PCBM and p-type P3HT exhibited both of the intrinsic electron and hole transport.

1. INTRODUCTION

Organic-inorganic lead halide based perovskite solar cells (PSCs) have seen a tremendous growth within a very small time frame and placed themselves respectfully in the efficiency table which can be gauzed by astonishing enhancement in the photoconversion efficiency (PCE) from 3.8% in 2009 to 22.1% in 2016[1,2] . Such a high efficiency PSCs bear ABX_3 structure, where A is monovalent cation typically consisted of organic methyl ammonium (MA) or Formamidinium ammonium (FA), B is bivalent cation which is primarily lead (Pb) and X is halide anion such as iodide (I-), bromide (Br-) and chloride (Cl-) etc.[3]. In spite of very high efficiency already attained by PSCs based on $MAPbI_3$ and $FAPbI_3$ perovskites resulting from long range balanced electron-hole diffusion lengths and high absorption coefficients, currently environmental toxicity because of Pb has become a considerable topic of debate in the material science community[4]. Therefore, with the time seeking for relatively more environment friendly solar cells, bivalent tin (Sn) and germanium (Ge) are being thought for the replacement of the Pb[5,6]. Recently, perovskites with non-typical ABX_3 structures such as $A_3Bi_2I_9$[7-9] have also been emerged as a new candidate not only as Pb free solar cells but also owing to its relatively better environmental and thermal stability. Thermal stability of the conventional Pb based PSCs (300^0C for bulk and 150-200^0C for thin films)[10] is an important issue, which is due to organic cation part and can be sorted out by replacing organic cation with metal cation such as cesium (Cs)[10,11]. Therefore, the replacement of MA^+ with Cs^+ and Pb^{2+} with Sn^{2+} seems to be an amicable solution for the toxicity as well as thermal stability issues of the most commonly utilized $CH_3NH_3PbX_3$ perovskites. Cs based perovskite $CsSnI_3$ exhibits high mobility and has been reported to be a good hole transporting material in solid state DSSCs as well as a good light harvester in PSCs[11,12]. However, the Sn prefers the tetravalent state, after Sn^{2+} based perovskite structure undergoes uncontrolled oxidation to form Sn^{4+} which simultaneously decomposes also in

ambient conditions leading to hampered efficiency of solar cells[13]. Therefore, synthesis of an air stable and Sn deficient perovskite structure (Cs_2SnI_6) was proposed by Lee et al in order to solve the issues such as air stability of $CsSnI_3$ and Pb toxicity[14]. It has been demonstrated that that Cs_2SnI_6 has band gap of 1.26 eV and exhibits Sn^{4+} state which is more stable against oxidation compared to Sn^{2+}. Following the synthesis, the material was used successfully in all solid state dye sensitized solar cells (SS-DSSCs) as a hole transport material with different dyes such as N719 and Z907. It was confirmed that pristine Cs_2SnI_6 exists as n-type semiconductor which changes to p-type after doping with Sn^{2+} and possess high electron and hole mobility of 310 cm^2/V.s and 42 cm^2/V.s, respectively, for n-type and p-type polycrystalline pellets sintered at 200^0C as measured by Hall effect. Therefore, noticing high mobility and favorable band gap, Cs_2SnI_6 motivated us to investigate further about the physical and interfacial properties of the thin films prepared and explore the application potential of Cs_2SnI_6 as a light absorber.

Photophysical parameters such as electron and hole mobility, electron and hole diffusion length, excitation carrier lifetime, mobile charge carrier lifetime are important material properties which often change after formation of interfaces with different materials which must be clearly understood before their utilization as an active photovoltaic material. Despite of the use of Cs_2SnI_6 as a hole transporter, the quantitative information on the charge transfer at the interface of different n-type and p-type semiconductor is still lacking and need an in-depth investigation. Recently, Saparov et.al[15] reported characterization and thin film formation of Cs_2SnI_6. They claimed that film formation by one-step solution processable spin coating leads to poor film coverage with CsI impurities, hence they implemented a two-step evaporation technique inside the nitrogen-filled glove box. N-type nature for the films formed by this method was confirmed

by Hall measurement having electron mobility of ~3 $cm^2/V.s$ and also they completely ruled out for the possibility of p-type doping in Cs_2SnI_6, which is we think need to be confirmed again.

In this article, we would like to report about the thin film formation of Cs_2SnI_6 by solution processed spray deposition technique. The existence of CsI impurity in this method was also noticed as reported earlier and was eliminated by improvising the solution process method[15]. Cs_2SnI_6 thin film formation and its morphology was checked by X-ray diffraction (XRD) and scanning electron microscopy (SEM) respectively. The well-known electron acceptor (EA) [6,6]-phenyl-C61-butyric acid methyl ester (PCBM)[16-18] and hole acceptor (HA) poly(3-hexylthiophene-2,5-diyl)(P3HT)[19-22] was utilized for investigating the interfacial charge transfer and recombination dynamics. We implemented conventionally used spectroscopic techniques namely photoluminescence (PL)[23-25] for excitation carrier lifetime, microwave photoconductivity (MPC)[26] for mobile charge carrier decay, transient absorption study such as femto-second (fs-TA) and nano-second (ns-TA)[23-34] for charge transfer occurring in femto-second (10^{-15} s) and nano-second (10^{-9} s) time regimes respectively. These kinds of techniques have been used successfully in solar cells such as DSSCs[30, 32, 33], Quantum-dot (QD) SSCs[34], Organic solar cells[31] and Pb based conventional PSCs[23-29] for understanding the charge transfer and recombination processes involved. The main aim of this work was to evaluate the electron and hole mobility inside Cs_2SnI_6 and also the possibility of photo excited charge carrier separation with the implementation of electron and hole extracting layers, which is very important for a light harvester in solar cell application.

2. EXPERIMENTAL SECTION

2.1 Materials and methods

Cs_2SnI_6 powder synthesis was the initial step before the sample preparation for different studies which was synthesized as per the earlier report[14]. Synthesis involves the mixing of aqueous HI (57% in H_2O, 7.1 ml) (TCI, Japan) with aqueous H_3PO_2 (50% in H_2O,1.7 ml) (Sigma Aldrich) under Ar atmosphere. SnI_2 (372 mg, 1 mmol) (Kojundo chemical laboratory Co. LTD, Japan) was later added to the mixture and stirred at 120^0C using an oil bath forming hot yellow solution of $HSnI_3$. In the next step, CsI (260 mg, 1 mmol) (Sigma Aldrich) powder was added to the solution which precipitates to form yellow needle shaped crystals. This precipitate was then dissolved in acetone (10 ml) (Wako, Japan) forming a red solution which was allowed to cool and left for 20-24 hours under Ar atmosphere resulting in to black colored crystals of Cs_2SnI_6. Finally the crystals formed were filtered and washed with ethanol (Wako, Japan). In the current study a solution (300 mg/ml) in dimethylformamide (DMF) (Sigma Aldrich, Japan) was used in all cases for sample preparation. Poly (3-hexylthiophene-2,5-diyl) (P3HT)(regioregular 99%, 10 mg/ml) (Sigma Aldrich, Japan) and [6,6]-phenyl-C61-butyric acid methyl ester (PCBM) (10 mg/ml) (Sigma Aldrich, Japan) solutions were prepared in 1,2 dichlorobenzene (Sigma Aldrich) for thin film fabrication.

2.2 Characterization

a) X-ray diffraction (XRD) Study - X-ray diffraction analysis (RINT-Ultima III, Rigaku, Japan) was performed in the range 10^0-60^0 for all of the thin films fabricated.

b) Hall Effect (HE) measurement – Van der pauw geometry was formed by sputtering the titanium (Ti~ 150 nm) and platinum (Pt~ 30nm) on the glass substrate of size 1 cm* 1cm.

c) Microwave photoconductivity decay (MPCD) - The MPCD system (LTA-1510EP) made by KOBELCO Co. Ltd was used for the measurement. A 349 nm laser and differential 26 GHz microwave antenna detection was implemented in the current study.

d) Scanning electron microscopy (SEM) The surface morphology of the samples was observed through scanning electron microscope (JEOL, Neoscope JCM-6000).

2.3 Optical characterizations

a) Absorption spectrum was measured by UV-visible-NIR spectrophotometer (V-570, JASCO, Japan) with an accuracy of ±1.5 nm. The optical instrument consists of double beam system with single monochromator in the wavelength 190 ~ 2500 nm with Halogen lamp (300 ~ 2500 nm) as light source.

b) Photoluminescence measurements were performed using the compact NIR photoluminescence lifetime spectrometer C12132 (HAMAMATSU, Japan) which is designed for measuring photoluminescence (PL) spectrum and PL lifetime in the NIR region (up to 1400 nm). Laser beam of wavelength 532 nm with 11.5 mW power, pulse width < 1 ns and repetition rate around 15 kHz was used to excite the samples.

Sample preparation - Glass slide (2 cm x 2 cm) (1.5 mm thick) was washed carefully with detergent water, distilled water, acetone and isopropanol for 5 minutes each. Thin film was formed by spray coating on the glass as shown in Figure 1. The spray machine (Iwata Custom micron, Japan) with nozzle system (0.23 mm matched head system) was used in the current study.

c) Photoelectron yield spectroscopy (PYS)- BUNKO-KEIKI, KV205-HK was employed for determining the ionization potential or highest occupied molecular orbital (HOMO) energy level

of the material. The synthesized powder was used for evaluation. Measurement was done in high vacuum condition (~ 10^{-4} Pa). The system consists of three parts; a monochromator, a measurement chamber, and a preparation chamber. Monochromatic light from a deuterium (D) lamp is introduced into a measurement chamber resulting in to photoelectron emission which is assisted by the external field and detected by a sub-pico ammeter.

2.4 Transient Absorption (TA) Measurements (Charge transfer analysis) - Two kinds of pump and probe transient absorption (TA) measurements known as fs-TA and ns-TA were implemented for the charge transfer studies[27, 34, 35]. A titanium/sapphire laser (CPA-2010, Clark-MXR Inc.) with a wavelength of 775 nm (0.4 mW), a repetition rate of 1 kHz, and a pulse width of 150 fs was used as the excitation source in the fs-TA measurement. This laser was separated into pump beam (wavelength tunable from 290 nm to 3 μm) using optical parametric amplifier (OPA) (a TOAPS from Quantronix) and probe beam (a white light). The pump wavelength of 650 nm was used in the current work for exciting Cs_2SnI_6 only. The time-resolved absorption spectra induced by the pump beam absorption in the samples could be obtained in the wavelength range of 660 nm - 910 nm. Then, the transient absorption kinetics at probe wavelength of 710 nm and 900 nm were analyzed, corresponding to the optical absorption peak and edge of Cs_2SnI_6, respectively. For the ns-TA measurement, the samples were also pumped at 650 nm using an optical parametric oscillator (OPO) (Panther, Continuum, Electro-Optics Inc.) excited by a Nd:YAG (Surelite II-10FR) based nanosecond pulsed laser (pulse width is 5 ns and repetition rate is 1 Hz). The transient absorption kinetics in samples was probed at 940 nm by a light coming from a fiber coupled CW semiconductor laser. All the measurements were carried out in N_2 atmosphere.

Sample preparation - Thin film samples were prepared by spray deposition method as shown schematically in the Figure 1. Three kinds of samples were prepared such as Cs_2SnI_6, Cs_2SnI_6 with PCBM (Cs_2SnI_6/PCBM) and Cs_2SnI_6 with P3HT (Cs_2SnI_6/P3HT). In case of Cs_2SnI_6/PCBM, PCBM was spin coated on the top of sprayed Cs_2SnI_6 at 3000 rpm for 10 sec. For coating P3HT on the sprayed Cs_2SnI_6, 2000 rpm was used for 10-15 sec and coated film was kept at room temperature for 3-4 hours followed by heating at 130^0C for 5 min. The absorption spectra of all the films fabricated is shown in SI-Figure 1.

3. RESULTS AND DISCUSSION

Thin film fabrication of Cs_2SnI_6 is an important step for evaluating its overall physical properties. Cs_2SnI_6 thin film been previously fabricated via evaporation method utilizing a two-step method[15]. It was reported that thin film fabrication by solution processable method led to non-uniform coverage of the films which was attributed to its poor solubility in polar solvents such as ethanol, DMF etc. In this work, we fabricated the thin films by spray coating based solution process as schematically shown in the Figure 1. First a concentration of 300 mg/ml Cs_2SnI_6 in DMF was prepared, which is 6 times higher than solution concentration reported earlier[15]. Solution was prepared by using magnetic stirring for 3 hours at room temperature. It was found that dehydrated DMF was best suited for the solution preparation and small amount of water content led to not only the poor solubility of Cs_2SnI_6 but also to the decomposition and formation of white precipitates. Both of the spin coating and spray coating methods were employed for making the films. In both of the cases films were heated at 130^0C for 5 minutes for removal of solvent. Films prepared depicted black color of Cs_2SnI_6 within 1 minute of heating indicates fast crystallization process. The difference between the films formed by two methods can be seen from SEM image as shown in the Figure 2. Spin coating as reported earlier showed that most of

the part was left uncovered with dendritic morphology[15]. In contrary, spray deposition led to the uniform coverage of the film and thickness of the film can be controlled by controlling the number of spray cycles.

The thin films fabricated were characterized by XRD as shown Figure 3. A perusal of the XRD pattern of Cs_2SnI_6 synthesized powder shown in the Figure 3(a) confirms the formation of pure material (space group of Fm-3m with unit cell parameter, a= 11.630 A^0). The pattern obtained was in good agreement with the previously published data[14, 15] as well as ICSD (22105) file for pure Cs_2SnI_6. Figures 3b & 3c is the XRD pattern for thin film formed by spray method. Observation from XRD pattern shows the formation of small crystallites in the film with the particle size of around 15 nm as calculated by employing the well-known Scherrer formula (supporting information (SI) Figure 2). The existence of small particles with 3-4 nm diameters along with big crystallites in the film prepared were also confirmed by TEM (SI- Figure 3). Thin film formed in Figure 3b contains CsI impurity which is similar to that observed previously by Saparov et al[15]. According to their report, the solution processable thin films have CsI impurities and can't be eliminated even by changing concentration and processing temperature. We think that Cs_2SnI_6 powder when dissolved in DMF possibly separated into two reactant parts such as CsI and SnI_4 because both of the material constitutes Cs_2SnI_6 also by employing a two-step method[15]. Therefore, the low melting point of SnI_4 (143^0C) results in to the increased probability of elimination of SnI_4 from the film prepared and will occur at even lower temperature (130^0C in the present case) due to increased surface area. The elimination of SnI_4 results in to the change in the stoichiometry and hence in formation of CsI impurity in the films thus prepared. This seems to be a plausible reason since treating the Cs_2SnI_6 film with CsI impurity with SnI_4 (100 mg/ml

ethanol) led to an CsI impurity free thin film as shown in Figure 3(c) because excess SnI_4 reacted with CsI to form Cs_2SnI_6.

Electronic absorption spectra of the thin film as shown in the Figure 4 exhibits similar behavior to that of the film prepared by thermal evaporation but the optical band gap (Eg) calculated for our film (1.54 eV) smaller than the previously reported values[15]. However, this value is larger than 1.27 eV as reported by Lee et.al[14]. The HOMO energy level of the material was measured to be at 5.3 eV (SI-Figure 4) below the vacuum level, which is again different than that reported previously[14, 15]. These differences in the values of the Eg and HOMO energy level were also seen previously in case of Sn based perovskites and this variation was mentioned due to different ways of making the material such as solution method, open and closed tube solid-state reaction methods[36]. This interesting phenomenon of variation let us to further insight into the optical properties of the films prepared in present case. Figure 5(a) shows the emission spectra in the wavelength region of 580-1030 nm where two distinct PL peaks around 710 nm and 885 nm were observed. This behavior could be originated from the existence of two different states within the same film. Two different band gap values due to presence of impurity can be easily ruled out because of the formation of impurity free thin films as evidenced by XRD investigations. Therefore, only another possibility is the occurrence of quantum effect for thin films containing the different sizes of quantum dots (QDs) with in the same material[31,36, 37]. At the same time, emission near to the optical absorption onset is commonly observed in case of QDs which is in agreement with the absorption peak at 710 nm[31, 37]. Therefore, we assign this peak to the quantum dot and the right peak appearing at 885 nm is assigned to the bulk part of the film. This observation in present research confirms that the films fabricated contain a mixture of bulk and QD parts. This observation also can be supported well by TEM image (SI-Figure 3)

obtained where small particles below 10 nm can be seen clearly and are probably the reason for quantum effect.

The transient PL decay was also measured as shown in Figures 5(b) and 5(c), where photo excitation carrier decay occurs in two steps. The initial fast decay occurs within 0.382±0.02 ns, while the second slower decay takes place in 32±2 ns period for the emission peak at 885 nm. The fast decay component can be attributed to the presence of defect or trap states in the material. Similarly, two-step decay was also observed at the emission wavelength of 710 nm, where both of the fast decays occurred within 0.60 ±0.09 ns and 0.71 ±0.02 ns. Because of very close decay times to each other, here we assume that there is only one decay process in this case. If we suppose that the QDs are mixed in the bulk film, then the decay of the PL intensity at 710 nm can also be resulted due to the electron transfer from the QDs into the bulk films. It can thus be concluded that the values of carrier decay and diffusion length obtained by PL lifetime measurement are apparently close to the respective values of conventional Pb based perovskite materials described elsewhere as summarized in the Table 1[23].

For a material to function as light absorber, physical properties such as carrier concentration, nature of the material, excitation carrier decay, diffusion length and mobile charge carrier life time play a crucial role to demonstrate its potential[23-28]. Table 1 lists the comparative values for Cs_2SnI_6 film prepared in the present work along with its previous reports and Pb based perovskite materials. About the nature of the material, both n-type and p-type was reported for the polycrystalline pellets sintered at 200^0C with electron and hole mobility value of 42 cm^2/Vs and 310 cm^2/Vs, respectively[14]. But some reports claimed for n-type nature only with electron mobility of 2.9 cm^2/Vs[15]. This difference could be again due to the difference in method of preparation of the material[36]. For our Cs_2SnI_6 thin films, we found the p-type nature when

evaluated by Hall measurement with carrier density of 3.65 x 10^{19} cm^{-3} and high hole mobility of 3.82 x 10^2 cm^2/Vs. Hole diffusion length value was then calculated to be 0.06 μm using fast carrier decay time and 5.5 μm with slow decay time. These calculated results are supported by the strong evidence of implementing Cs_2SnI_6 as a hole transporter in earlier reports[38]. MPCD monitors directly the mobile charge carrier population in the material and for conventional Pb based materials it is more than 1 μs[26]. In our material this value was around 0.310 ± 0.02 μs as shown in Figure 5(d) which supports for the charge separation or exciton splitting within Cs_2SnI_6, but this value will be different with the change in crystal size. The physical properties measured and listed in Table 1 clearly support the suitability of Cs_2SnI_6 to be used as an absorber. Recently few reports also came with utilization of Cs_2SnI_6 as light absorbing layer[39, 40]. Although the initial performances of devices are less than 1% but results are highly encouraging and supports the properties evaluated in present study as well. Apart from charge transport behavior within the material, for fabricating the solar cell, the interfacial contacts with different materials also play a crucial role and this analysis would be helpful for further enhancing the solar cell performances.

Interfacial charge transfer studies have been performed taking PCBM and P3HT interface with Cs_2SnI_6 in to consideration using TA measurement. Figure 6 shows the typical charge transfer processes involved in perovskite based solar cells along with the their approximate time durations of occurrence. In this present work, PCBM and P3HT have been taken as representative electron transport and hole transport materials. In order to have in-depth insight about the interfacial charge transfer processes, three types of the samples were taken in to consideration and related energy band diagrams have been shown in the Figure 7. Cs_2SnI_6 film deposited on glass has thickness of about 600-800 nm which was measured through the cross-sectional SEM image as shown in the SI-Figure 4. The laser pump of 650 nm was used to excite

the Cs_2SnI_6 only, as confirmed by SI-Figure 1, so that signals corresponding to charge transfer at the interface can be observed clearly. The time-resolved TA spectra of PCBM only, P3HT only and Cs_2SnI_6 only films deposited is shown in SI- Figure 6, where pump light was incident from glass side. The absence of TA signals in case of PCBM only and P3HT only further confirms the selective excitation of Cs_2SnI_6 only. For Cs_2SnI_6 only film deposited a clear bleaching signal around 700 nm was observed, which corresponds to the optical absorption peak shown in Figure 4. From optical absorption spectra, a band gap of 1.54 eV has been calculated. But the bleach signal of 700 nm corresponds to the photon energy of 1.77 eV, different from 1.54 eV. Therefore, this bleaching signal at 700 nm (1.77 eV) might be associated with the QDs (corresponding PL peak of 710 nm), and the 1.54 eV (wavelength: 805 nm) could be assigned to the band gap of the bulk film (corresponding PL peak of 885 nm). Apart from the bleaching signal, an excited state absorption around 900 nm was also obtained as shown in the Figure 8 and SI-Figure 6(c). The TA signals decay faster for the Cs_2SnI_6 film deposited with P3HT or PCBM compared to that of Cs_2SnI_6 film alone when the pump light was incident from the interfaces of Cs_2SnI_6 /P3HT or Cs_2SnI_6/PCBM. These results indicate a successful electron or hole transfer from Cs_2SnI_6 to PCBM or to P3HT. The fs-TAS kinetics reveals a charge transfer dynamics in the tens of ps time domain for all of the three samples at 900 nm as shown in Figure 8. The fs-TA response was well fitted with equation, $y = y0 + A1*\exp(-t/t1)$, where y0 is the final value of transient absorption, t1 is the decay time. The excitation carrier decay of 4.85 ±0.65 ps was obtained in case of Cs_2SnI_6 only when film was pumped from the film side. When combined with P3HT and PCBM, the decay was faster with values of 3.45 ±0.21 ps and 3.15 ±0.20 ps, respectively. This fast decay in absorption signal is indication for the charge transfer at the donor/accepter interfaces and our results are also in accordance with that of previously reported systems[26-28]. This difference in

decay time could be also due to energy transfer[41], however in the present case possibility of energy transfer can be totally ruled out as there is no overlap of PL spectrum of Cs_2SnI_6 with PCBM and less than 10% with P3HT absorption spectrum, as shown in SI-Figure 7. Interestingly, there was no change in the absorption signals, when the Cs_2SnI_6 films were excited from the glass side (SI-Figure 8) suggesting that charge transfer time from the glass/Cs_2SnI_6 interface to the Cs_2SnI_6/P3HT interface or Cs_2SnI_6/PCBM interface may be larger than the measured time scale of 1 ns in fs-TA measurement. Also, it is important to note that all the charge transfer process involved are laser power independent as we realized the similar decay time for Cs_2SnI_6 film deposited (SI-Figure 6d).

It is well known that charge recombination process usually occurs in μs time scales and commonly analyzed by ns-TAS (Figure 6)[32]. The films were probed at NIR wavelength, which is useful for studying the recombination dynamics for the interfaces between excited film and charge collecting layer[26, 27]. Figure 9(a) and 9(b) show the difference in the TA signals obtained in all of the three cases (Figure 7). The TA decay can be fitted very well using a bi-exponential equation, Y= A1 exp(-t/t1) + A2 exp(-t/t2), where t1 and t2 are decay times of charge carriers with (A1/A1+A2)* 100 % and (A2/A1+A2)* 100 %, respectively. The values obtained from the fitting are listed in Table 2. The probe beam of 940 nm was used to monitor the photoexcited carriers in Cs_2SnI_6 and/or the holes in P3HT. Two long life-times of photoexcited carriers in Cs_2SnI_6 were observed, i.e., about 2μs and 20 μs. This result indicates that a part of the photoexcited carriers in Cs_2SnI_6 have lifetimes as long as in μs range. In the case of Cs_2SnI_6/P3HT a significant increase in the longer life-time was observed (from 20 μs to 110 μs), indicating a charge separation occurred at the Cs_2SnI_6/P3HT interface. Since the pump light of 650 nm only excited Cs_2SnI_6 not P3HT, it means that photoexcited holes could be injected from

Cs_2SnI_6 to P3HT at the interface. The recombination between the electrons in Cs_2SnI_6 and holes in P3HT was about 110 μs. In the case of Cs_2SnI_6/PCBM, there is no significant change in the TA decays with and without PCBM, which could be due to fast electron recombination at this interface. The similar observations were noticed when different concentrations of P3HT and PCBM were taken (SI- Figure 10). TA analysis, therefore, exhibits the presence of both of the electron and hole transports within the material, however, the hole transport is better within the material compared to the electron transport which can be well understood because of its p-type behavior.

4. CONCLUSION

In summary, a CsI impurity free thin films of Cs_2SnI_6 has been successfully fabricated by using spray deposition technique. P-type nature of the Cs_2SnI_6 along with the high mobility of 3.82 x 10^2 cm^2/Vs as estimated by Hall measurement assured its suitability as HTM for DSSCs. The Cs_2SnI_6 shows high absorption coefficient of 5 x 10^4 cm^{-1} which motivates for implementing it as an absorber layer also. Our finding based on PL and TEM investigations indicates the formation of quantum dot and bulk within the same film using this method. Excitation carrier decay time is very fast as confirmed by PL and TAS data, which could be due to the presence of defect or trap states. Excitation carrier life time needs to be increased for better performance of material as an absorber and, therefore, big particles or crystallite based film is needed to be formed or passivation of the films is highly desired. The ns-TAS results support the fast hole mobility inside Cs_2SnI_6 compared to electron mobility, which suggests for the need of good electron extracting layer to be coupled with Cs_2SnI_6. In order to achieve this, mesoporous structure with n-type semiconductors such as TiO_2, ZnO or SnO_2 could be an amicable choice for fast electron

transport. Another possibility could be the by implementation of bulk-heterojunction device architecture in combination with the electron transporter like PCBM.

Acknowledgements:

This research was supported by New Energy and Industrial Technology Development Organization (NEDO), Japan.

REFERENCE

1 Kojima, A.; Teshima, K.; Shirai, Y.; Miyasaka, T. Organometal Halide Perovskites as Visible-Light Sensitizers for Photovoltaic Cells. *J. Am. Chem. Soc.* **2009**, *131* (17), 6050–6051.

2 www.nrel.gov/ncpv/images/efficiency_chart. jpg

3 Green, M. A.; Ho-Baillie, A.; Snaith, H. J. The Emergence of Perovskite Solar Cells. *Nat. Photonics* **2014**, *8* (7), 506–514.

4 Eperon, G. E.; Stranks, S. D.; Menelaou, C.; Johnston, M. B.; Herz, L. M.; Snaith, H. J. Formamidinium Lead Trihalide: A Broadly Tunable Perovskite for Efficient Planar Heterojunction Solar Cells. *Energy Environ. Sci.* **2014**, *7* (3), 982.

5 Hao, F.; Stoumpos, C. C.; Cao, D. H.; Chang, R. P. H.; Kanatzidis, M. G. Lead-Free Solid-State Organic–inorganic Halide Perovskite Solar Cells. *Nat. Photonics* **2014**, *8* (6), 489–494.

6 Stoumpos, C. C.; Frazer, L.; Clark, D. J.; Kim, Y. S.; Rhim, S. H.; Freeman, A. J.; Ketterson, J. B.; Jang, J. I.; Kanatzidis, M. G. Hybrid Germanium Iodide Perovskite

Semiconductors: Active Lone Pairs, Structural Distortions, Direct and Indirect Energy Gaps, and Strong Nonlinear Optical Properties. *J. Am. Chem. Soc.* **2015**, *137* (21), 6804–6819.

7 Park, B. W.; Philippe, B.; Zhang, X.; Rensmo, H.; Boschloo, G.; Johansson, E. M. J. Bismuth Based Hybrid Perovskites $A_3Bi_2I_9$ (A: Methylammonium or Cesium) for Solar Cell Application. *Adv. Mater.* **2015**, *27* (43), 6806–6813.

8 Vigneshwaran, M.; Ohta, T.; Iikubo, S.; Kapil, G.; Ripolles, T. S.; Ogomi, Y.; Ma, T.; Pandey, S. S.; Shen, Q.; Toyoda, T.; et al. Facile Synthesis and Characterization of Sulfur Doped Low Bandgap Bismuth Based Perovskites by Soluble Precursor Route. *Chem. Mater.* **2016**, acs.chemmater.6b02315.

9 Singh, T.; Kulkarni, A.; Ikegami, M.; Miyasaka, T. Effect of Electron Transporting Layer on Bismuth-Based Lead-Free Perovskite $(CH_3NH_3)_3$ Bi_2I_9 for Photovoltaic Applications. *ACS Appl. Mater. Interfaces* **2016**, *8* (23), 14542–14547.

10 Eperon, G. E.; Paternò, G. M.; Sutton, R. J.; Zampetti, A.; Haghighirad, A. A.; Cacialli, F.; Snaith, H. J. Inorganic Caesium Lead Iodide Perovskite Solar Cells. *J. Mater. Chem. A* **2015**, *3* (39), 19688–19695.

11 Kumar, M. H.; Dharani, S.; Leong, W. L.; Boix, P. P.; Prabhakar, R. R.; Baikie, T.; Shi, C.; Ding, H.; Ramesh, R.; Asta, M.; et al. Lead-Free Halide Perovskite Solar Cells with High Photocurrents Realized through Vacancy Modulation. *Adv. Mater.* **2014**, *26* (41), 7122–7127.

12 Chung, I.; Lee, B.; He, J.; Chang, R. P. H.; Kanatzidis, M. G. All-Solid-State Dye-

Sensitized Solar Cells with High Efficiency. *Nature* **2012**, *485* (7399), 486–489.

13 Ogomi, Y.; Morita, A.; Tsukamoto, S.; Saitho, T.; Fujikawa, N.; Shen, Q.; Toyoda, T.; Yoshino, K.; Pandey, S. S.; Ma, T.; et al. $CH_3NH_3Sn_XPb_{(1-X)}I_3$ Perovskite Solar Cells Covering up to 1060 Nm. *J. Phys. Chem. Lett.* **2014**, *5* (6), 1004–1011.

14 Lee, B.; Stoumpos, C. C.; Zhou, N.; Hao, F.; Malliakas, C.; Yeh, C. Y.; Marks, T. J.; Kanatzidis, M. G.; Chang, R. P. H. Air-Stable Molecular Semiconducting Iodosalts for Solar Cell Applications: Cs_2SnI_6 as a Hole Conductor. *J. Am. Chem. Soc.* **2014**, *136* (43), 15379–15385.

15 Saparov, B.; Sun, J.-P.; Meng, W.; Xiao, Z.; Duan, H.-S.; Gunawan, O.; Shin, D.; Hill, I. G.; Yan, Y.; Mitzi, D. B. Thin-Film Deposition and Characterization of a Sn-Deficient Perovskite Derivative Cs_2SnI_6. *Chem. Mater.* **2016**, *28* (7), 2315–2322.

16 Xu, Z.; Chen, L.-M.; Chen, M.-H.; Li, G.; Yang, Y. Energy Level Alignment of poly(3-Hexylthiophene): [6,6]-Phenyl C[sub 61] Butyric Acid Methyl Ester Bulk Heterojunction. *Appl. Phys. Lett.* **2009**, *95* (1), 13301.

17 Liu, C.; Wang, K.; Du, P.; Yi, C.; Meng, T.; Gong, X. Efficient Solution-Processed Bulk Heterojunction Perovskite Hybrid Solar Cells. *Adv. Energy Mater.* **2015**, *5* (12), 1402024.

18 Chiang, C.-H.; Wu, C.-G. Bulk Heterojunction perovskite–PCBM Solar Cells with High Fill Factor. *Nat. Photonics* **2016**, *10* (3), 196–200.

19 Mihailetchi, V. D.; Xie, H. X.; de Boer, B.; Koster, L. J. a.; Blom, P. W. M. Charge Transport and Photocurrent Generation in Poly(3-Hexylthiophene): Methanofullerene Bulk-Heterojunction Solar Cells. *Adv. Funct. Mater.* **2006**, *16* (5), 699–708.

20 Kim, Y.; Choulis, S. A.; Nelson, J.; Bradley, D. D. C.; Cook, S.; Durrant, J. R. Device Annealing Effect in Organic Solar Cells with Blends of Regioregular poly(3-Hexylthiophene) and Soluble Fullerene. *Appl. Phys. Lett.* **2005**, *86* (6), 1–3.

21 Chirvase, D.; Parisi, J.; Hummelen, J. C.; Dyakonov, V. Influence of Nanomorphology on the Photovoltaic Action of Polymer–fullerene Composites. *Nanotechnology* **2004**, *15* (9), 1317–1323.

22 Padinger, F.; Rittberger, R. S.; Sariciftci, N. S. Effects of Postproduction Treatment on Plastic Solar Cells. *Adv. Funct. Mater.* **2003**, *13* (1), 85–88.

23 Stranks, S. D.; Snaith, H. J. Metal-Halide Perovskites for Photovoltaic and Light-Emitting Devices. *Nat. Nanotechnol.* **2015**, *10* (5), 391–402.

24 Stranks, S. D.; Eperon, G. E.; Grancini, G.; Menelaou, C.; Alcocer, M. J. P.; Leijtens, T.; Herz, L. M.; Petrozza, A.; Snaith, H. J. Electron-Hole Diffusion Lengths Exceeding 1 Micrometer in an Organometal Trihalide Perovskite Absorber. *Science* **2013**, *342* (6156), 341–344.

25 Xing, G.; Mathews, N.; Sun, S.; Lim, S. S.; Lam, Y. M.; Grätzel, M.; Mhaisalkar, S.; Sum, T. C. Long-Range Balanced Electron- and Hole-Transport Lengths in Organic-Inorganic $CH_3NH_3PbI_3$. *Science* **2013**, *342* (6156), 344–347.

26 Marchioro, a; Teuscher, J.; Friedrich, D.; Kunst, M.; van de Krol, R.; Moehl, T.; Gratzel, M.; Moser, J. E. Unravelling the Mechanism of Photoinduced Charge Transfer Processes in Lead Iodide Perovskite Solar Cells. *Nat. Photonics* **2014**, *8* (3), 250–255.

27 Shen, Q.; Ogomi, Y.; Chang, J.; Toyoda, T.; Fujiwara, K.; Yoshino, K.; Sato, K.;

Yamazaki, K.; Akimoto, M.; Kuga, Y.; et al. Optical Absorption, Charge Separation and Recombination Dynamics in Sn/Pb Cocktail Perovskite Solar Cells and Their Relationships to Photovoltaic Performances. *J. Mater. Chem. A* **2015**, *3* (17), 9308–9316.

28 Ponseca, C. S.; Savenije, T. J.; Abdellah, M.; Zheng, K.; Yartsev, A.; Pascher, T.; Harlang, T.; Chabera, P.; Pullerits, T.; Stepanov, A.; et al. Organometal Halide Perovskite Solar Cell Materials Rationalized: Ultrafast Charge Generation, High and Microsecond-Long Balanced Mobilities, and Slow Recombination. *J. Am. Chem. Soc.* **2014**, *136* (14), 5189–5192.

29 Ponseca, C. S.; Hutter, E. M.; Piatkowski, P.; Cohen, B.; Pascher, T.; Douhal, A.; Yartsev, A.; Sundström, V.; Savenije, T. J. Mechanism of Charge Transfer and Recombination Dynamics in Organo Metal Halide Perovskites and Organic Electrodes, PCBM, and Spiro-OMeTAD: Role of Dark Carriers. *J. Am. Chem. Soc.* **2015**, *137* (51), 16043–16048.

30 Brauer, J. C.; Marchioro, A.; Paraecattil, A. a.; Oskouei, A. a.; Moser, J.-E. Dynamics of Interfacial Charge Transfer States and Carriers Separation in Dye-Sensitized Solar Cells: A Time-Resolved Terahertz Spectroscopy Study. *J. Phys. Chem. C* **2015**, *119* (47), 26266–26274.

31 Borchert, H. Elementary Processes and Limiting Factors in Hybrid Polymer/nanoparticle Solar Cells. *Energy Environ. Sci.* **2010**, *3* (11), 1682.

32 Miguel, G. De; Cohen, B.; Organero, J. A.; Pandey, S.; Hayase, S.; Douhal, A. Real-Time Photodynamics of Squaraine-Based Dye-Sensitized Solar Cells with Iodide and Cobalt Electrolytes. **2013**.

33 Pandit, B.; Luitel, T.; Cummins, D. R.; Thapa, A. K.; Druffel, T.; Zamborini, F.; Liu, J. Spectroscopic Investigation of Photoinduced Charge-Transfer Processes in FTO/TiO_2/N719 Photoanodes with and without Covalent Attachment through Silane-Based Linkers. *J. Phys. Chem. A* **2013**, *117* (50), 13513–13523.

34 Sato, K.; Ono, K.; Izuishi, T.; Kuwahara, S.; Katayama, K.; Toyoda, T.; Hayase, S.; Shen, Q. The Effect of CdS on the Charge Separation and Recombination Dynamics in PbS/CdS Double-Layered Quantum Dot Sensitized Solar Cells. *Chem. Phys.* **2016**, *478*, 159–163.

35 Shen, Q.; Ogomi, Y.; Chang, J.; Tsukamoto, S.; Kukihara, K.; Oshima, T.; Osada, N.; Yoshino, K.; Katayama, K.; Toyoda, T.; et al. Charge Transfer and Recombination at the Metal oxide/$CH_3NH_3PbClI_2$/spiro-OMeTAD Interfaces: Uncovering the Detailed Mechanism behind High Efficiency Solar Cells. *Phys. Chem. Chem. Phys*. **2014**, *16* (37), 19984–19992.

36 Stoumpos, C. C.; Malliakas, C. D.; Kanatzidis, M. G. Semiconducting Tin and Lead Iodide Perovskites with Organic Cations: Phase Transitions, High Mobilities, and near-Infrared Photoluminescent Properties. *Inorg. Chem.* **2013**, *52* (15), 9019–9038.

37 Son, D. I.; Kwon, B. W.; Park, D. H.; Seo, W. S.; Yi, Y.; Angadi, B.; Lee, C. L.; Choi, W. K. Emissive ZnO-Graphene Quantum Dots for White-Light-Emitting Diodes. *Nat Nanotechnol*. 2012, pp 465–471.

38 Kaltzoglou, A.; Antoniadou, M.; Kontos, A. G.; Stoumpos, C. C.; Perganti, D.; Siranidi, E.; Raptis, V.; Trohidou, K.; Psycharis, V.; Kanatzidis, M. G.; et al. Optical-Vibrational Properties of the Cs_2SnX_6(X=Cl,Br,I) Defect Perovskites and Hole-Transport Efficiency in Dye-Sensitized Solar Cells. *J. Phys. Chem. C* **2016**, *120* (22), 11777–11785.

39 Qiu, X.; Jiang, Y.; Zhang, H.; Qiu, Z.; Yuan, S.; Wang, P.; Cao, B. Lead-Free Mesoscopic Cs_2SnI_6 Perovskite Solar Cells Using Different Nanostructured ZnO Nanorods as Electron Transport Layers. *Phys. status solidi - Rapid Res. Lett.* **2016**, *10* (8), 587–591.

40 Qiu, X.; Cao, B.; Yuan, S.; Chen, X.; Qiu, Z.; Jiang, Y.; Ye, Q.; Wang, H.; Zeng, H.; Liu, J.; et al. From Unstable $CsSnI_3$ to Air-Stable Cs_2SnI_6: A Lead-Free Perovskite Solar Cell Light Absorber with Bandgap of 1.48eV and High Absorption Coefficient. *Sol. Energy Mater. Sol. Cells* **2017**, *159*, 227–234.

41 Huang, J.-S.; Goh, T.; Li, X.; Sfeir, M. Y.; Bielinski, E. A.; Tomasulo, S.; Lee, M. L.; Hazari, N.; Taylor, A. D. Polymer Bulk Heterojunction Solar Cells Employing F{ö}rster Resonance Energy Transfer. *Nat. Phot.* **2013**, 7, 479-485.

Table1. Comparison table with existing lead (Pb) based perovskite

	Previous Reports on Cs_2SnI_6 (p-type) [14]	**Previous Reports on Cs_2SnI_6 (n-type)** [14, 15]	**Cs_2SnI_6 (p-type) calculated in current work**	**Previous Reports on $CH_3NH_3PbI_{3-x}Cl_x$ and $CH_3NH_3PbI_3$** [23-25, 28]	
Electron/hole concentration	1×10^{14}	(1×10^{14}), (6×10^{16})	3.65×10^{19}	$10^{15} \sim 10^{20}$	[cm^{-3}]
Hole Mobility	42	_	3.82×10^{2}	(~2.16)	[$cm^2V^{-1}s^{-1}$]
Electron Mobility	–	(3.10×10^{2}) , (2.9)	–	(~1.68)	[$cm^2V^{-1}s^{-1}$]
Excitation Life time (Photoluiminescence) ,τ1	–	–	0.381	(100~2000)	nano second (ns)
τ2	–	–	~32	–	nano second (ns)
Diffusion Length (Using τ1)	–	–	0.06	(1~ 3)	micro meter (μm)
Diffusion Length (Using τ2)	–	–	5.5	–	micro meter (μm)
Mobile charge carrier life time, (Microwave Photoconductivity decay)	–	–	~310	>1000	nano second (ns)

Table 2. Fitting results obtained after the ns-TAS

Sample	**t1 (μs)**	**t2 (μs)**	**A1**	**A2**	**A1/(A1+A2)**	**A2/(A2+A1)**
Cs_2SnI_6	2.3±0.2	20±2	0.18	0.04	82%	18%
Cs_2SnI_6/P3HT	2.5±0.1	110±1	0.36	0.08	82%	18%
Cs_2SnI_6/PCBM	1.6±0.1	10±1	0.28	0.098	74%	26%

Figures and captions

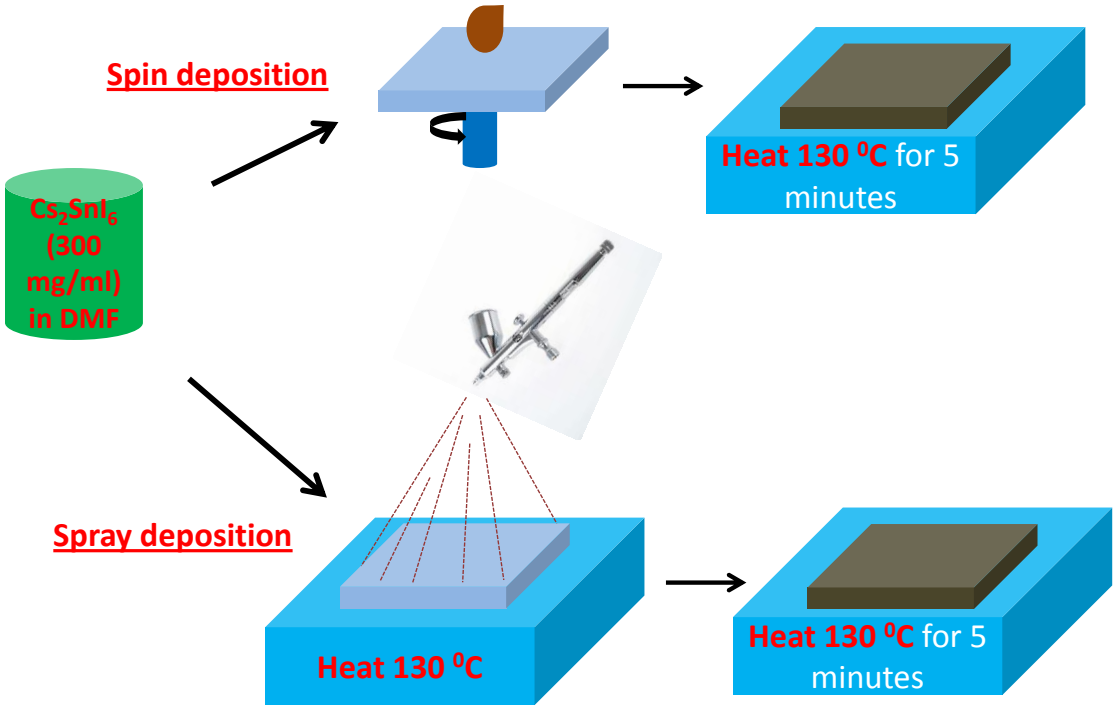

Figure 1. Schematic showing the fabrication of thin films

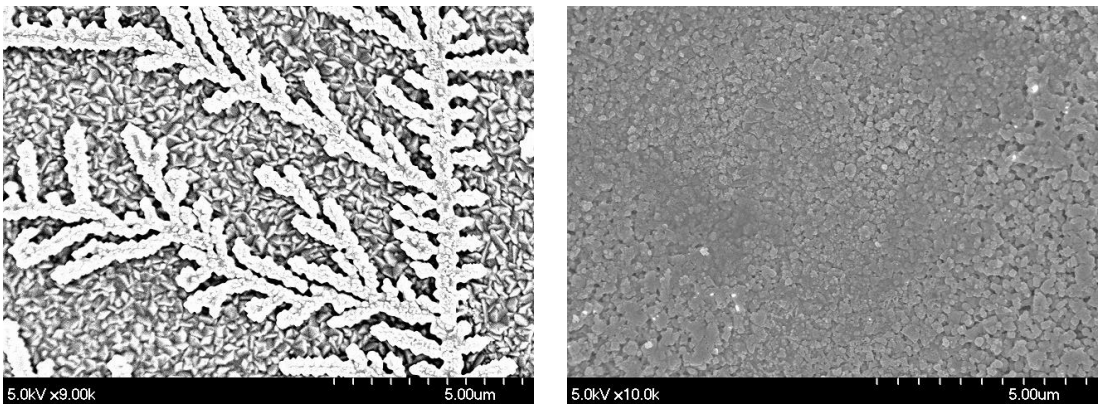

(a) **(b)**

Figure 2. SEM image for (a) spin coated film (b) spray coated film

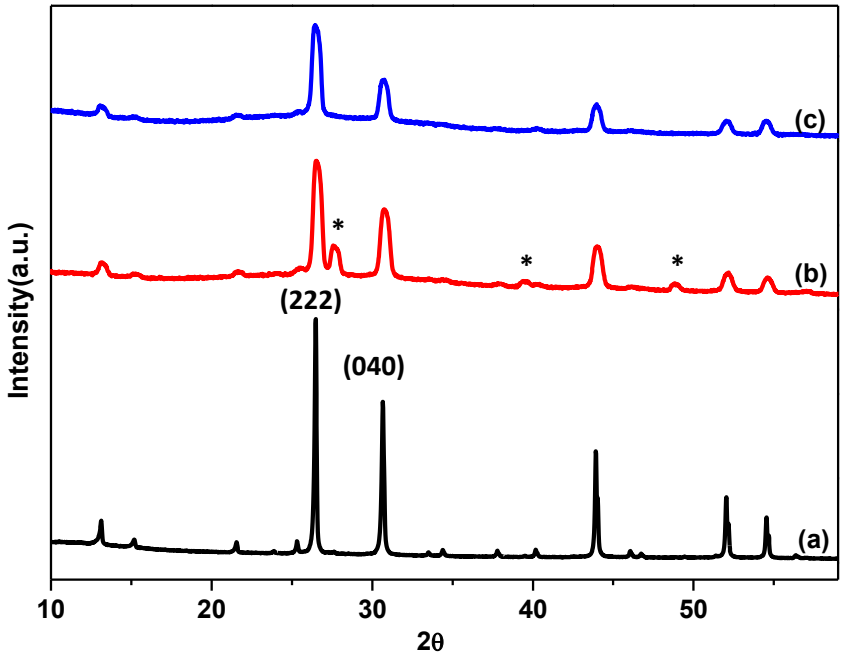

Figure 3. XRD pattern for Cs_2SnI_6 (a) powder synthesized (b) thin film containing CsI impurity (*) (c) thin film without any impurity

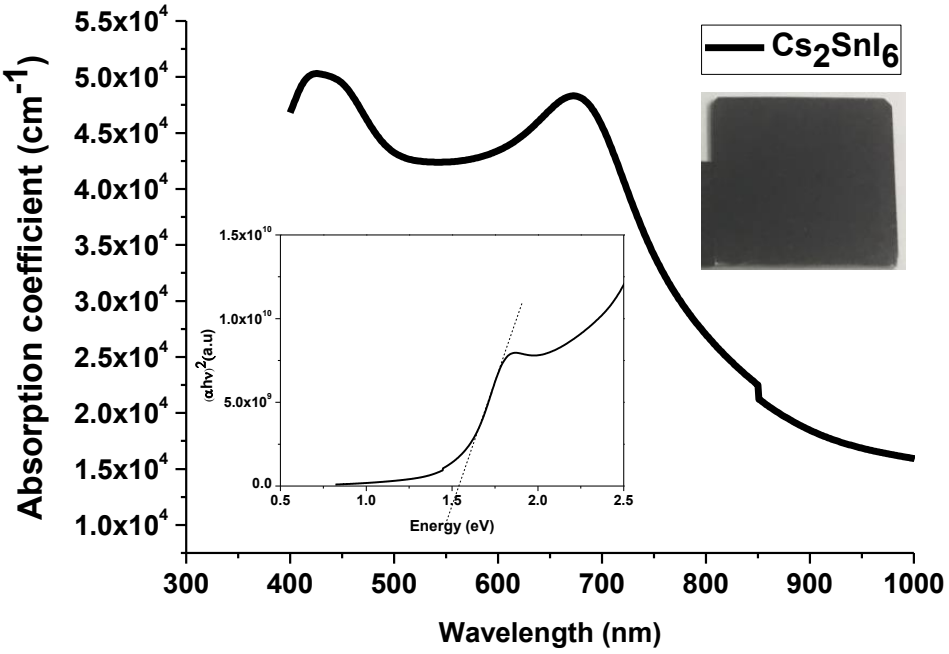

Figure 4. Absorption coefficient for Cs_2SnI_6, inset shows the band gap calculated.

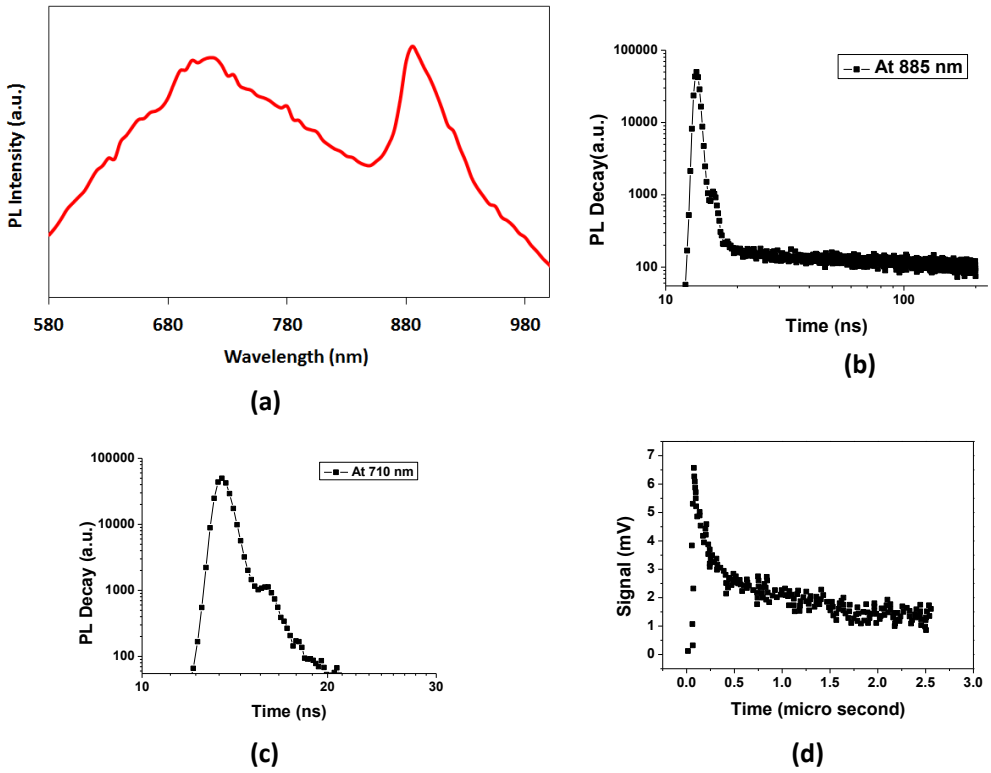

Figure 5. (a) PL emission spectra obtained, (b) PL decay at 885 nm, (c) PL decay at 710 nm and (d) MPCD for Cs_2SnI_6 films

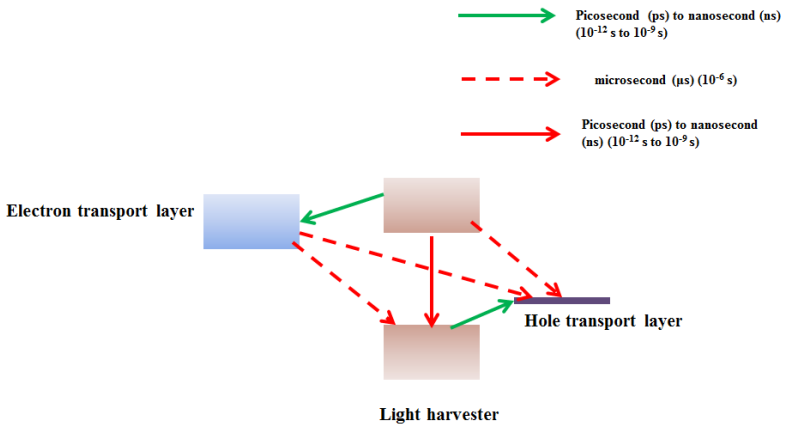

Figure 6. Schematic diagram showing the different charge transfer process with approximate time of occurrence in conventional perovskite materials

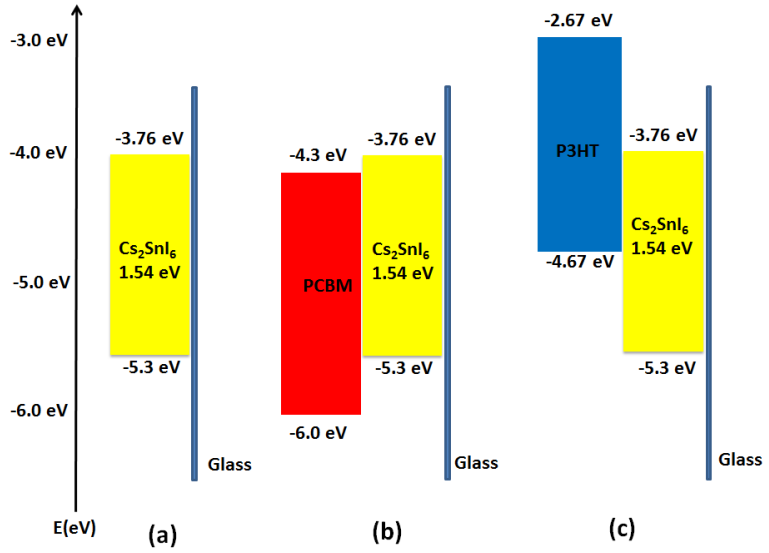

Figure 7. Sample used for TAS study (a) Cs_2SnI_6 only (b) Cs_2SnI_6 with PCBM (c) Cs_2SnI_6 with P3HT

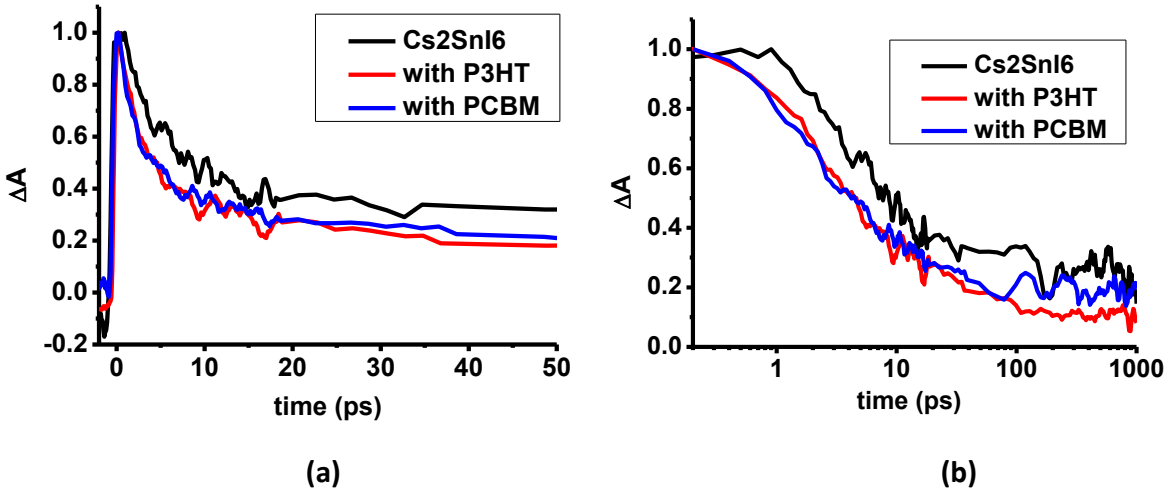

Figure 8. fs-TA decay for different samples pumped at 650 nm and probed at 900 nm from film side

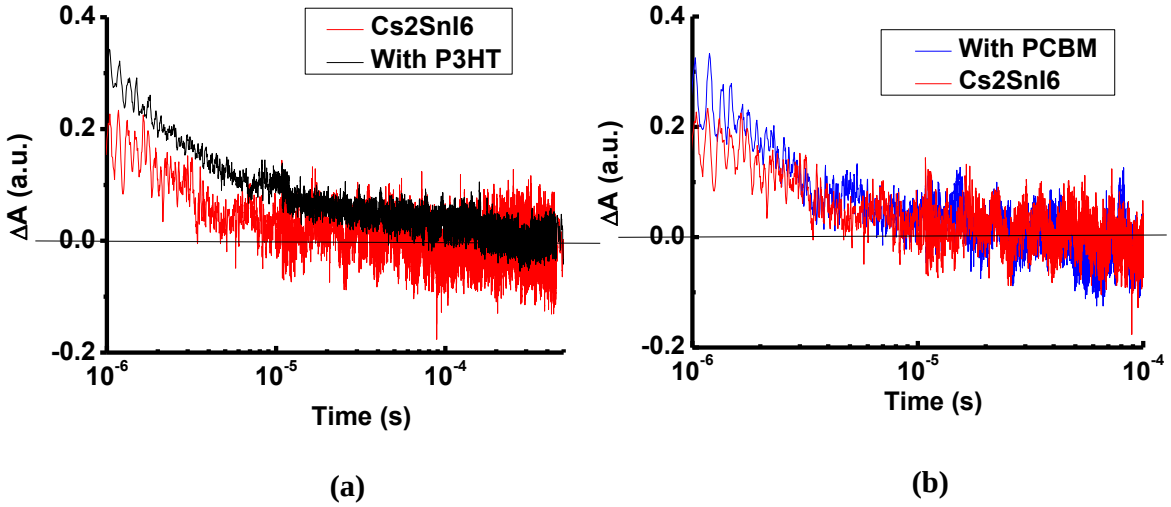

Figure 9. ns-TA decay for different samples pumped at 650 nm and probed at 940 nm from glass side